Simple Model for Describing and Estimating Wind Turbine Dynamic Inflow

Knudsen, Torben; Bak, Thomas

Published in:
American Control Conference (ACC), 2013

Publication date:
2013

Document Version
Publisher's PDF, also known as Version of record

2013 American Control Conference (ACC)
Washington, DC, USA, June 17-19, 2013

Simple Model for Describing and Estimating Wind Turbine Dynamic Inflow.

Torben Knudsen and Thomas Bak

***Abstract*— Wind turbines operate with sudden change in pitch angle, rotor or wind speed. In such cases the wake behind the turbine, achieve steady state conditions only after a certain delay. This phenomenon is commonly called dynamic inflow. There are many models for dynamic inflow. The most accurate use a method that can be characterised as the blade element momentum method plus a dynamic equation for the induction factor. This method then needs calculations along the blade for a number of sections including numerical solution of equations. This is numerical demanding. The simplest models amounts to placing a lead-lag filter after rotor torque and thrust calculated from static tables of the power and thrust coefficients. The filter constants will then vary with average wind speed. The filtered versions of torque and thrust are then an approximate modelling of the dynamic inflow. The dynamic inflow model suggested here places itself in between the most complex and the most simple both in accuracy, numerical demands and physical appeal. The suggested models behavior is demonstrated by simulation and the usefulness for extended Kalman filtering is assessed both via simulated data and real full scale turbine data.**

I. Introduction

Dynamic inflow (DI) modelling has normally been ignored in connection with control design. A very common approach in wind turbine control engineering is to assume the gains from blade pitch to be given as the gradient found from the power coefficient, C_p function. This function is really based on blade element momentum (BEM) theory which is a static model and the DI is consequently ignored.

There has been research on DI for wind turbines the last 20 years. Still, only one reference indicating a successful usage for control design [1]. Here a simple lead lag linear transfer function is used as a filter where the input is the static rotor torque or thrust and the output should then be the torque or thrust accounting for the DI. This is a rather simple black box type model. Also very complicated models based on BEM theory are suggested e.g. in [2]. These can be categorized as first principles or white box models.

The above models seems to be either to simple or to complex for wind turbine control.

The complex are too nonlinear and numerical demanding and the simple do not describe the behavior accurately enough.

In the following a model is presented which is a compromise in both complexity, physical interpretability and accuracy.

Torben Knudsen and Thomas Bak is with section of Automation and Control, Aalborg University, Fredrik Bajers Vej 7C2-212 DK-9220 Aalborg, Denmark tk@es.aau.dk

First the aerodynamics including DI is introduced. This is followed by a discussion leading to the suggested simplification. The expected qualitative behavior for the simplified model are verified by simulations where it is compared to a model with no DI included. A quantitative success criteria is that the one step output prediction errors (also called residuals) from a model including DI is smaller than the one step output prediction errors from a similar model without DI. To produce the predictions needed for this an extended Kalman filter (EKF) is developed. The prediction error assessment is made for both simple simulation model data and for full scale experimental data. Notice that the EKF has a significant value on its own as it also estimates the *effective wind speed* (EWS) which is used for single turbine control [3]–[6].

The main contributions are: 1) The simplified DI model. 2) The extended Kalman filter which also estimates EWS. 3) The assessment on full scale experimental data.

II. Aerodynamic modelling

The aerodynamic forces on a blade section is given by the local wind velocity i.e. the wind speed and angle of attack as illustrated in figure 1. To be able to relate to the physical

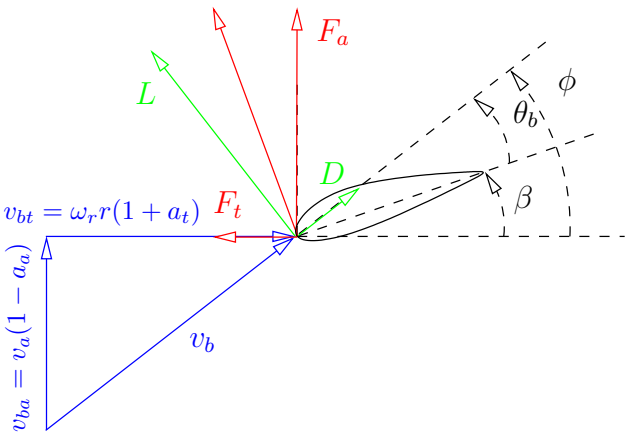

Fig. 1. Illustration of basic aerodynamics for a wind turbine blade section at radius r.

environments the turbine is placed in, it is standard to use the ambient wind speed v_a which can be interpreted as the wind speed which is at the turbine location if the turbine was not there. The local velocity seen by a blade section at radius r has the speed v_b

$$v_b = \sqrt{v_{ba}^2 + v_{bt}^2}\,, \tag{1}$$

978-1-4799-0176-0/$31.00 ©2013 AACC

$$v_{ba} = v_a(1 - a_a) \ , \ v_{bt} = \omega_r r(1 + a_t) \ , \tag{2}$$

where a_a and a_t are axial and tangential induction factors. The angle of attack θ_b is

$$\theta_b = \phi - \beta \ , \tag{3}$$

$$\phi = \arctan\left(\frac{v_{ba}}{v_{bt}}\right) \ , \tag{4}$$

where β is the blade pitch angle and ϕ is the local inflow angle. The axial F_a and tangential F_t forces per length on the blade section is then given from the lift C_l and drag C_d coefficients

$$F_a = \cos(\phi)L + \sin(\phi)D \ , \tag{5}$$

$$F_t = \sin(\phi)L - \cos(\phi)D \ , \tag{6}$$

$$L = \frac{1}{2}\rho v_b^2 c C_l(\theta_b) \ , \ D = \frac{1}{2}\rho v_b^2 c C_d(\theta_b) \tag{7}$$

where ρ is air density and c is the blade cord length.

The total thrust and torque from the rotor can now be calculated by integrating the above over the rotor. When rotor speed ω_r, pitch angle β and ambient wind speed v_a is given there are still the induction factors a_a and a_t missing. Using stationary values found from BEM theory [2], the the total stationary forces on the rotor can be conveniently expressed by the precalculated C_p and C_t tables which only depends on pitch and tip speed ratio λ as follows

$$T_{r,s} = \frac{1}{2}\rho v_a^3 A C_p(\lambda, \beta)\frac{1}{\omega_r} \ , \tag{8}$$

$$F_{r,s} = \frac{1}{2}\rho v_a^2 A C_t(\lambda, \beta) \ , \tag{9}$$

$$\lambda = \frac{\omega_r R}{v_a} \ , \tag{10}$$

The inductions can also be tabulated but in contrast to C_p and C_t the induction also depends on the local radius r

$$a_a = A_a(\lambda, \beta, r) \ , \tag{11}$$

$$a_t = A_t(\lambda, \beta, r) \ . \tag{12}$$

All the above, however, only holds under stationary flow conditions which are given by ω_r, pitch angle β and ambient wind speed v_a. These signals will typically vary smoothly and slowly compared to the aerodynamic time constant which is often approximated by

$$\tau = \frac{3D}{2v_m} \ , \tag{13}$$

where a typical value would be $\tau = 3\ 90/2/10 = 13.5$ sec. Rotor speed and ambient wind speed varies slowly due to rotor inertia and inertia in the wind mass flow, but pitch angle can vary very quickly because of powerful actuators e.g. 10 deg/sec can easily be achieved. For these fast pitch variations the dynamic inflow becomes significant especially close to rated wind speed. The necessary modelling suggested by many authors [2], [7]–[9] is to include a first order dynamic model governing the changes in induction coefficients at radius r as follows

$$\dot{a}_f = \frac{1}{\tau(v_m)}(a_s - a_f) \ , \tag{14}$$

where a_s is the stationary values from the tables and a_f are the filtered dynamic values used in the calculation of v_b and θ_b and the rest of the many calculations leading to the rotor forces. This model is complex and numerical demanding. At every time sample and for every blade section from root to tip the BEM calculations has to be performed including the dynamic induction (14) which is specific for a section. This also means that the model structure is expanded with as many states as there are blade sections e.g. 3×10 to cover the dynamic inductions.

III. A SIMPLIFIED DYNAMIC INFLOW MODEL

The ambition is to simplify compared to the above BEM based method but still base it on physics. Furthermore it would be practical if it could work as an addition to the simple static model based only on C_p and C_t table.

In figure 2 the situation where the pitch is suddenly moved towards higher power is illustrated. The vectors shown are the static solutions which can be found from tables. Assume the ambient wind speed is constant and that the stationary situation is the blue one. Then the pitch instantaneously jumps to the red position. At this instant the blue flow will still persist and give a higher angle of attack with increased forces and power. After a while the flow will change from blue to red with increased inductions. Using stationary aerodynamics means that the flow changes instantly from blue to red.

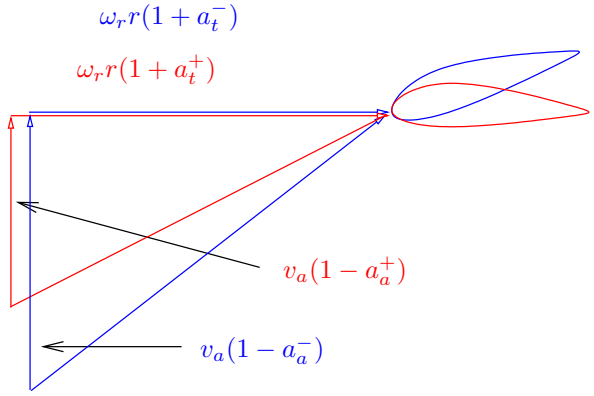

Fig. 2. Illustration of dynamic inflow from a fast pitch change from blue to red. The vectors are stationary speeds before in blue and after the change in red.

The change in tangential induction a_t is ignored for simplicity and as it is assumed less important compared to the axial induction a_a i.e. $a_t^- \sim a_t^+$. Then the static red wind flow just after the change can be turned into the dynamic blue one by introducing the "fictive" ambient wind speed v_f given by

$$v_f = v_a \frac{1 - a_a^-}{1 - a_a^+} \ , \tag{15}$$

To avoid doing more than one calculation one rotor radius r_e is used to represent all sections of the blade. This gives the following equations for including the DI in the calculations

of rotor torque and thrust

$$\lambda = \frac{\omega_r R}{v_a} \tag{16a}$$

$$a_s = a_a(\lambda, \beta) \tag{16b}$$

$$\tau = \frac{3D}{2v_m} \tag{16c}$$

$$\dot{a}_f = \kappa(a_s - a_f)\ ,\ \kappa = \frac{1}{\tau} \tag{16d}$$

$$v_f = v_a \frac{1 - a_f}{1 - a_s} \tag{16e}$$

$$T_r \sim \frac{1}{2}\rho v_f^3 A C_p(\lambda, \beta)\frac{1}{\omega_r} \tag{16f}$$

$$F_r \sim \frac{1}{2}\rho v_f^2 A C_t(\lambda, \beta) \tag{16g}$$

Essentially this means that the only change to models ignoring dynamic inflow is the introduction of the fictive ambient wind speed v_f given by (16d)–(16e). However, above not only C_p and C_t are used, which are standard, but also the additional table with the induction a_a is needed 16b. This table is normally possible to extract from the (BEM) software calculating C_p and C_t. To avoid this and make the model even simpler, actuator disc theory gives the following induction factor approximation:

$$C_t = 4a(1-a) \wedge 0 \leq a \leq \frac{1}{2} \Leftrightarrow \tag{17}$$

$$a = \frac{1}{2}\left(1 - \sqrt{1 - C_t}\right)\ . \tag{18}$$

Then a can be calculated directly from the C_t table by using (18) in place of (16b). This will work for normal pitch to feather turbines where a will be in the range $[0, \frac{1}{3}]$ in non stalled operation.

IV. Simulation studies

To test if the above DI model gives the expected behavior, the behavior of a simulated turbine with and without the DI is studied. The widely used NREL 5MW virtual turbine [10] is ideal for this purpose. This turbine serves as a test turbine for many investigation and a Simulink version has been developed which is useful here. The Simulink version has a "standard" complexity which is suitable for control purposes. It consist of static aerodynamics using C_p and C_t tables and the mechanics include two inertia drive train and tower fore aft dynamics. The pitch and generator torque actuators are modelled with simple first order models. For control there is a controller developed by NREL. More details can be found in [10], [11] and [12]. A second version of this Simulink NREL 5MW has been made with the simple DI included as described above in (16) and (18).

To test the qualitative behavior two test cases are selected. The first case is where the significance of DI is expected to be largest. This is close to rated wind speed where C_p is flat and the static rotor torque does not change much. Including dynamic inflow should then show a relatively larger change in rotor torque. The second case is where the pitch is larger and the C_p is not so flat. Here a relatively smaller change is expected when including the dynamic inflow. These two cases are shown in the figures 3–4 below. The figures shows the results of simulations with constant wind speed and a pitch angle stepping between two values. In this way it is easier to see the principal behavior compared to cases with fluctuating wind.

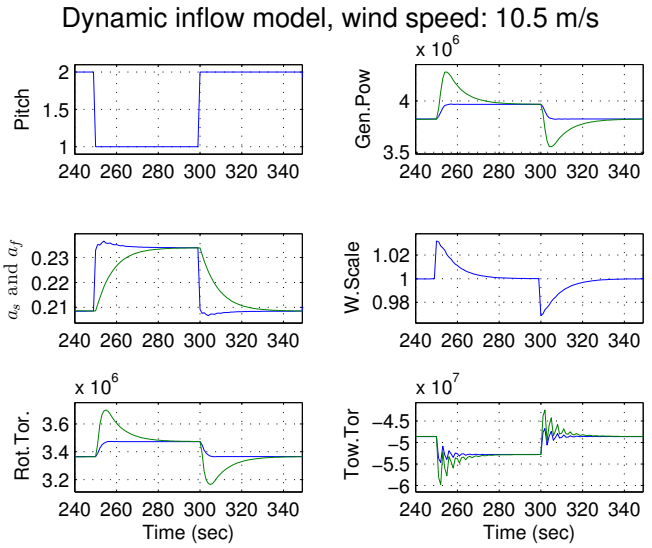

Fig. 3. Simulation close to rated wind speed with constant wind and stepping pitch angle. In the plots the blue line is without dynamic inflow and the green is with dynamic inflow except in the plot of induction factors where blue is the static and green is the filtered induction factor. W.Scale is the wind scaling factor in (16e), Rot.Tor is the rotor torque and Tow.Tor is the tower tilting torque.

As expected figure 3 shows that dynamic inflow has a significant effect when operating close to rated. Clearly the main shaft torque and the tower torque oscillations increase which will add to fatigue when including DI. However, a significant effect for normal operation in varying wind can not be concluded from this. Figure 4 shows only little effect as the induction is low for high pitch angles. This behavior is in good agreement with the full scale experimental test made earlier [13].

V. Experimental validation methods

An appealing and intuitive way to make quantitative validation is to make pitch steps on a real turbine and simulate the same steps with the model. If the results compare well the model is validated. This is the approach taken in [14], [15]. The disadvantages with the step response approach is that it is not easy to get access to pitch step experiments on standard industrial size turbines, this has not been possible for this investigation. Further, step responses are only possible below rated power where the pitch are not reserved for speed control. Also it is difficult, actually impossible, to expose the model to exactly the same wind field as the real turbine.

A second method is to use a high fidelity turbine simulator in place of the real wind turbine. This is certainly an option which has the advantage that it gives access to signals which are not measurable for real turbines as e.g. induction factors

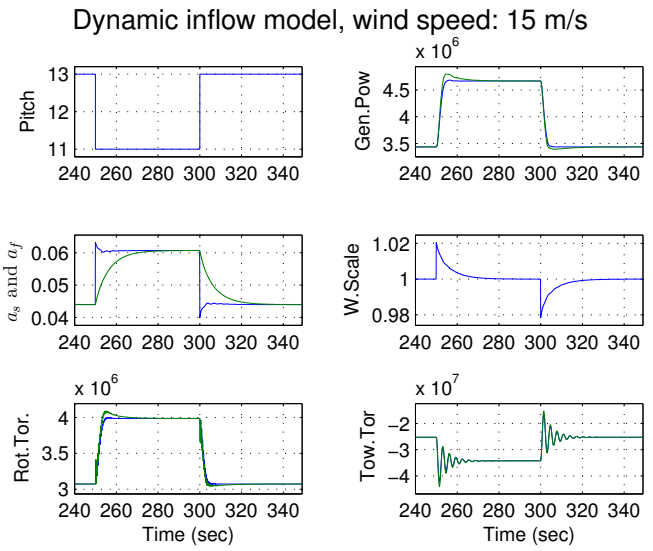

Fig. 4. Simulation for wind speed 15 m/s and average pitch at 12 deg. Otherwise similar to figure 3.

and EWS. However, the problem is to what extend the turbine simulator fits reality regarding the investigated model issue.

A third method is to use data from a real turbine in normal operation where data are easier to obtain. Then it is not possible to directly measure signals like induction factors and EWS. The only way is to evaluate model performance by prediction capability: if adding a model component reduces the optimal output prediction errors the component should be added.

This last approach will be used here. As the models involved has non linearities a truly optimal predictor does not exist. The best predictor is obtained by an EKF. This will also provide useful state estimates for e.g. EWS and the induction factor.

VI. Extended Kalman filter

The EKF is based on a state space model. For convenience all the needed equations are collected in (19) starting with the state dynamics and ending with the static relations. The separate equations are described in detail below.

$$I_r\dot{\omega}_r = T_r - T_g \ , \tag{19a}$$

$$M_n\ddot{d}_n = F_r - k_t d_n - d_t\dot{d}_n \ , \tag{19b}$$

$$\dot{v}_t = -\gamma(v_m)v_t + n_1 \ , \tag{19c}$$

$$\dot{v}_m = n_2 \ , \tag{19d}$$

$$\dot{a}_f = \kappa(v_m)(a_s - a_f) \ , \tag{19e}$$

$$\kappa(v_m) = \frac{2v_m}{3D} \ , \tag{19f}$$

$$\gamma(v_m) = \frac{\pi v_m}{2L} \ , \tag{19g}$$

$$V_1(v_m) = \frac{\pi v_m^3 t_i^2}{L} \ , \tag{19h}$$

$$v_r = v_t + v_m - \dot{d}_n \ , \tag{19i}$$

$$v_f = v_r\frac{1-a_f}{1-a_s} \ , \tag{19j}$$

$$a_s = \frac{1}{2}\left(1 - \sqrt{1 - C_t(\lambda,\beta)}\right) \ , \tag{19k}$$

$$T_r = \frac{1}{2}\rho v_f^3 A_r C_p(\lambda,\beta)\frac{1}{\omega_r} \ , \tag{19l}$$

$$F_r = \frac{1}{2}\rho v_f^2 A_r C_t(\lambda,\beta) \ , \tag{19m}$$

$$\lambda = \frac{\omega_r R_r}{v_r} \ , \tag{19n}$$

$$T_g = \frac{p}{\mu\omega_r} \ . \tag{19o}$$

The mechanical part is quite standard and are discussed in several text books [16], [17]. It is relatively simple and consists of a one inertia drive train (19a) where I_r is total inertia and a one degree of freedom tower for aft part (19b) where M_n is total nacelle mass and d_n is nacelle/tower displacement.

The wind model is important for the estimator and is not standard. It is however well described in [3]. In brief, v_t (19c) is the turbulence and v_m (19d) is the slower (mean) part of the wind. The turbulence part is time varying by the dependence on v_m both in dynamics (19g) and incremental variance (19h). The parameters in the wind model are fixed with turbulence intensity $t_i = 0.1$, turbulence length scale $L = 170.1$ and incremental variance off n_2 V_2= 2^2/600. Notice that the only process noise entering the model is the noise driving the wind states (19c) and (19d). The term "incremental variance" is really for the corresponding Wiener process in a proper stochastic formulation but it still measures the size of the variation. For more details on stochastic differential equations and Wiener processes see, e.g. [18, sec. 10-1].

The DI inflow part (19e), (19j) and (19k) is new while the rest of the aerodynamics (19l)– (19n) is standard except that the fictive wind v_f is used for rotor torque and thrust. Finally, the generator torque T_g is given by (19o) where p is the generator power and μ is the efficiency.

The measurement part (20) simply adds white measurement noise to the rotor speed ω_r, the wind speed seen by the nacelle v_r and the nacelle acceleration a_n.

$$\omega_m = \omega_r + v_1 \ , \tag{20a}$$

$$v_n = v_r + v_2 \ , \tag{20b}$$

$$a_m = a_n + v_3 \ . \tag{20c}$$

The state space model with state, input and output is given below in condensed form.

$$x = \begin{bmatrix}\omega_r & \dot{d}_n & d_n & v_t & v_m & a_f\end{bmatrix}^\intercal \ , \tag{21}$$

$$u = \begin{bmatrix}\beta & p\end{bmatrix}^\intercal \ , \tag{22}$$

$$y = \begin{bmatrix}\omega_m & v_n & a_m\end{bmatrix}^\intercal \tag{23}$$

Notice that the noise enters linearly as shown in (24).

$$\dot{x} = f(x,u) + n \ , \tag{24a}$$

$$y = h(x,u) + v \tag{24b}$$

Notice that pitch and generator power are considered to be noise free inputs as these normally are very precise. This means that the only parameter left is the measurement variance for the measurements in (20). This depends on the specific wind turbine.

The EKF is implemented as a continuous discrete EKF. The details can be found in [3].

VII. Proof of concept from simulated NREL 5MW data

As stated in section V the final validation is done using real data. However, in contrast to a KF, the EKF can not be proven to be neither optimal nor stable. Therefore it makes sense to start by proofing the concept on a simple simulation model before using real data. For this a Simulink model of the NREL 5MW virtual turbine has been used. The simulator is a Simulink implementation of the mathematical model (19) in section VI except it is a two inertia model instead of the one inertia model in (19a). The turbine is controlled by the controller supplied by NREL. For details on the specific NREL 5MW turbine refer to to [10]. The measurement noise v_1, v_2, v_3 in (20) are simulated as independent white noise with the standard deviations 0.01, 2, and 0.01 for rotor speed, nacelle wind speed and tower fore aft acceleration respectively. This amount to approximately 1% of nominal speed, 2m/s wind and 4% of standard deviations on tower accelerations. Experience with real multi MW machines tells that these are reasonable values. The sampling rate is set to 10 Hz as this is a typical value used for the turbine main controller. The mean wind speed is chosen as 10.5 m/s as this covers the switching region where there are pitching activity close to minimum pitch. Here the induction factor is the highest and the changes largest which results in the most pronounced effect of dynamic inflow. The inputs and outputs used by the EKF are shown in figure 5.

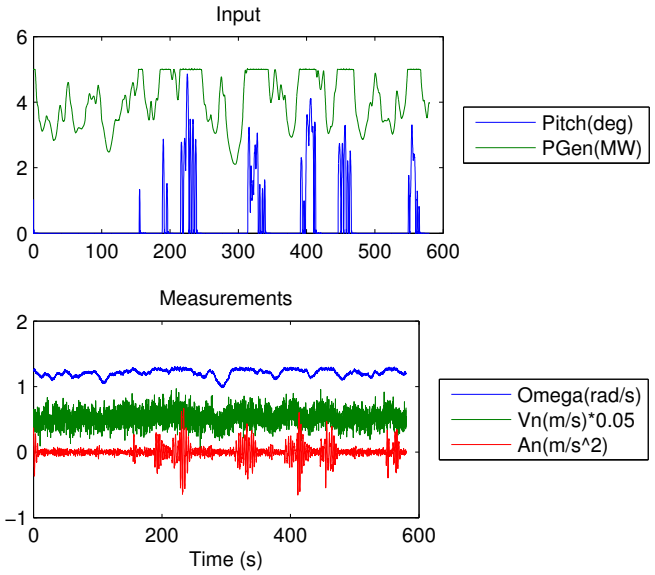

Fig. 5. Simulated data for NREL 5MW virtual turbine for mean wind speed 10.5 m/s.

Using these data it is possible to obtain good results with the EKF. As seen in the figure there is good excitation of both pitch and generator power. In this case the residuals will only be white noise if the model used for the EKF is perfect and the non-linearities do not spoil the optimality of the EKF too much. As seen in figure 6 only residuals related to the acceleration does not pass the whiteness test. Notice that the reason for not passing this test is the large number of samples, 5220, not because the auto correlations are large. Notice though that there have been simulations, especially at higher wind speeds, where these residual tests where not as convincing.

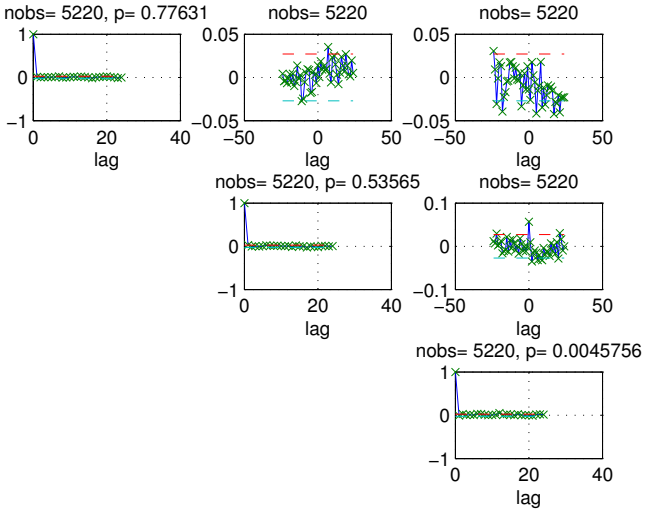

Fig. 6. Output prediction errors auto correlations based on NREL5MW simulated data. The "p" in the plot is a p-value from a Portmanteau whiteness test [19].

It has also been verified that the residuals decreases when including useful model component. The EKF has been made in 3 versions one based on the model described in section VI i.e. a one inertia model including tower and DI, one where DI is not included and one where neither DI nor tower is included. The resulting root mean squares (RMS) values are seen in table I. In the first tree columns it is seen that the RMS for residuals is only reduced very little. In contrast the EWS is reduced 12% by including the tower and further 22% by including DI which is a substantial improvement. Also notice, that RMS on EWS can only be assessed because this is a simulation where the "real" EWS is available.

Model	Omega	Nac WS	T. Acc	EWS
One I, Tower, DI	0.0108	2.04	0.0156	0.3370
	(1.00)	(1.00)	(1.00)	(1.00)
One I, Tower	0.0109	2.06	0.0172	0.429
	(1.01)	(1.01)	(1.10)	(1.27)
One I,	0.0111	2.07		0.489
	(1.03)	(1.01)		(1.45)

TABLE I

RMS output prediction errors based on NREL5MW simulated data samples 581:5800. The figures in parenthesis is normalised with the top row.

VIII. Validation from measured NREL CART3 data

This investigation has benefited from having data from the NREL CART3 turbine including all necessary parameters for the EKF. This turbine is of medium size at 600 Kw with a rotor diameter of 40 m and a hub height of 34.7 m. The turbine has been selected because it is large enough to be useful and it is a non commercial turbine with no confidentiality issues. Also there has been plenty of different data sets to choose between. All of them last for 300 second with is sufficient even though longer series would be nice. For more information about the turbine see [20]. The original data is sampled at 400 Hz which is down sampled to 10 Hz using appropriate anti aliasing filters.

The model, which the EKF is based on, covers frequencies up to and including the tower frequency around 0.9 Hz. Above this frequency the data, especially generator speed, has a significant spectral peak at the 3P frequency 1.85 Hz where P is the rotation frequency. This peak is removed by filtering all data by a second order notch filter. A much smaller peak is also seen at the drive train frequency 2.7 Hz. Furthermore, the acceleration signal is detrended and the wind speed measurement is scaled to fit the meteorology mast wind speed on average. Finally, the site measured air density 1.00 is used instead of the standard 1.22 Kg/m^3. This is important as the rotor torque otherwise will be over estimated by 22%. The resulting data, which will be used for the EKF, is shown in figure 7. Notice that the the wind turbine is operating on and above rated wind speed such that there is a good pitching activity at low pitch values where the effect of dynamic inflow is must pronounced.

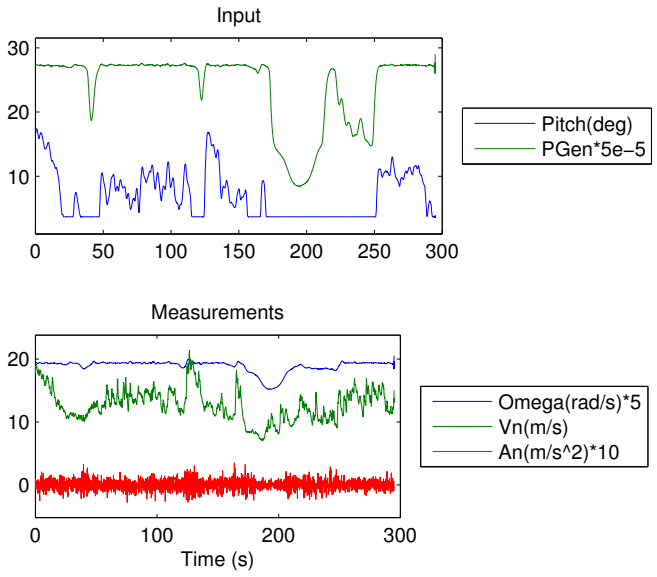

Fig. 7. Input output data for NREL CART3 turbine.

Data was filtered with exactly the same EKF as was used for the NREL 5MW data in section VII. However, the filter could only process half of the data before going unstable. For this first half of the data the RMS on acceleration errors where more than 3 times the expected value calculated by the EKF. Therefore the measurement standard deviation on accelerations where increased from 0.01 m/s^2 used for NREL 5MW data to 0.07 which made the EKF performance better and the RMS on residuals more in line with the expected. Notice that this one parameter change was the only necessary to make the EKF used for the NREL 5MW data work for the CART3 data.

The results from EKF of the CART3 data are seen below. The autocorrelations using the full model including one inertia drive train, tower and DI is shown in figure 8. Clearly, the residuals are not as white as for the simulated NREL 5MW data in figure 6. The residuals for rotor speed and tower accelerations are not too far from white noise even though there are both fast and slow variations. The residuals for the wind speed differs significantly from white noise which is also expected as this is a very disturbed measurement of wind speed.

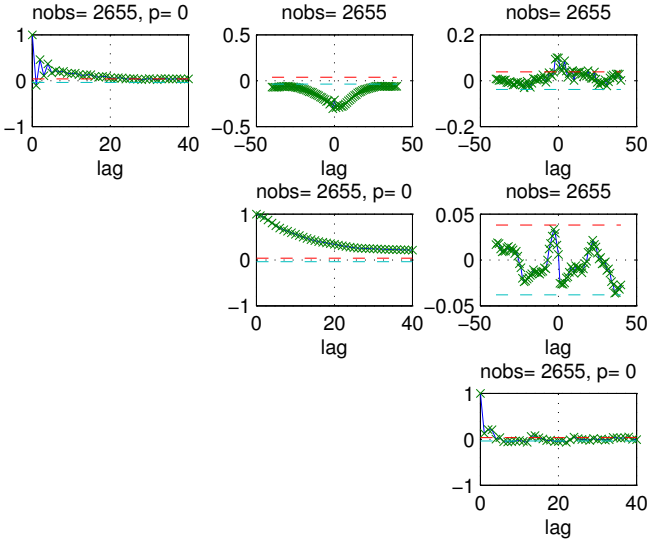

Fig. 8. Output prediction errors auto correlations based on NREL CART3 data for roor speed, wind speed and accelerations.

The RMS values for residuals from the EKF based on the tree different models are seen in table II. Clearly there is no significant difference so none of the models turns out to be superior. Based on this the dynamic inflow model suggested here can not be proven to be a significant model component but neither can it be claimed to be “wrong”. Notice that this is actually similar to the picture for NREL 5MW simulation data. And for these data the improvement for EWS was significant even though the improvement for EKF residuals was not.

After all, the induction factor is the new component in this work. Therefore it is concluded as shown in figure 9 that the induction factor estimate at least is high when the pitch is low and visa verse as it is supposed to.

IX. Conclusion

A new simplified model for dynamic inflow is presented. It is demonstrated by simple simulation of a NREL 5MW

Model	Omega	Nac WS	T. Acc
One I, Tower, DI	0.00899	1.10	0.0799
	(1.00)	(1.00)	(1.00)
One I, Tower	0.00860	1.14	0.0782
	(0.96)	(1.04)	(0.98)
One I,	0.00861	1.13	
	(0.96)	(1.03)	

TABLE II

RMS OUTPUT PREDICTION ERRORS BASED ON CART3 DATA SAMPLES 296:2950. THE FIGURES IN PARENTHESIS IS NORMALISED WITH THE TOP ROW.

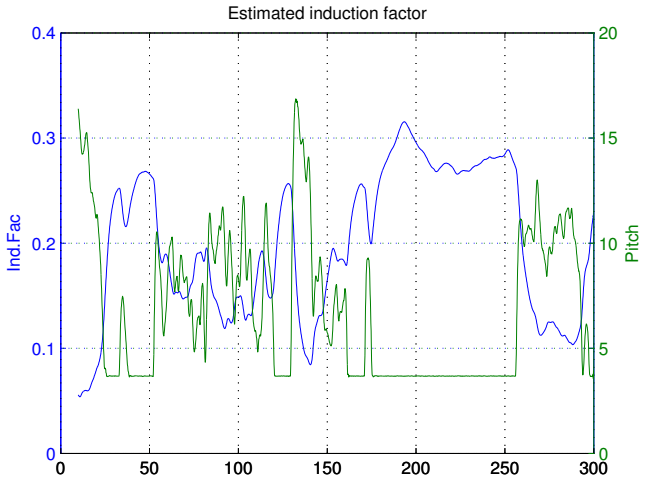

Fig. 9. Estimated induction factor and blade pitch angle.

virtual turbine that it behaves in accordance with the expected and with pitch step responses measured on real turbines reported in the literature. The assessment is done by comparing RMS for residuals from the EKF based on a model with and without the dynamic inflow component. Based on data from the simple simulations it is possible to show that the EKF works and gives slightly smaller RMS on residuals when the dynamic inflow component is included. For the simulated data the RMS on effective wind speed estimation error can also be calculated and this improved significantly. The same assessment is made based on real data from the NREL CART3 turbine. Here there were no clear effect of including the dynamic inflow judged from the measurement residual RMS. Notice that this is not to different from the simulated results where the improvement were very small. Comparing based on effective wind speed can unfortunately only be done from simulated data as the effective real wind speed can not be measured precisely. Based on this the dynamic inflow model suggested here, can not be proven useful for real data but neither does it prove to be wrong.

ACKNOWLEDGEMENT

Thanks to Paul Fleming from NREL for supplying the data for CART3.

This work was supported by the Danish Ministry of Science and Innovation under the scope of Project CASED - Concurrent Aeroservoelastic Analysis and Design of Wind Turbines

This work has been partly funded by Norwegian Centre for Offshore Wind Energy (NORCOWE) under grant 193821/S60 from Research Council of Norway (RCN). NORCOWE is a consortium with partners from industry and science, hosted by Christian Michelsen Research.

REFERENCES

[1] T. Van Engelen and E. Van der Hooft, "Dynamic inflow compensation for pitch controlled wind turbines," in *European Wind Energy Conference 2004*, 2004.

[2] M. O. L. Hansen, *Aerodynamics od Wind Turbines*, 2nd ed. Earthscan, 2008.

[3] T. Knudsen, M. Soltani, and T. Bak, "Prediction models for wind speed at turbine locations in a wind farm," *Wind Energy*, vol. 14, pp. 877–894, 2011, published online in Wiley Online Library (wileyonlinelibrary.com). DOI: 10.1002/we.491.

[4] W. Qiao, W. Zhou, J. M. Aller, and R. G. Harley, "Wind speed estimation based sensorless output maximization control for a wind turbine driving a dfig," *IEEE Transactions on Power Electronics*, vol. 23, no. 3, pp. 1156–1169, 2008.

[5] K. Z. Østergaard, P. Brath, and J. Stoustrup, "Estimation of effective wind speed," in *Journal of Physics: Conference Series 75*, EWEA. IOP Publishing, 2007.

[6] W. Leithead, "Effective wind speed models for simple wind turbine simulations," in *BWEA 1992*, 1992, pp. 321–326.

[7] J. D. Sørensen and J. N. Sørensen, Eds., *Wind Energy Systems - Optimising design and construction for safe and reliable operation*, ser. Woodhead Publishing Series in Energy. Woodhead Publishing, 2011, no. 10.

[8] N. N. Sørensen and H. A. Madsen, "Modelling of transient wind turbine loads during pitch motion," in *Proceedings of the European Wind Energy Conference 2006*, Milan, May 2006.

[9] S. Øye, "Tjæreborg wind turbine, 5. dynamic inflow measurement," Technical University of Denmark, Lyngby, Denmark, Tech. Rep. VK-233, 1992.

[10] J. Jonkman, S. Butterfield, W. Musial, and G. Scott, "Definition of a 5-mw reference wind turbine for offshore system development," National Renewable Energy Laboratory, 1617 Cole Boulevard, Golden, Colorado, USA, Tech. Rep. NREL/TP-500-38060, 2009.

[11] J. D. Grunnet, M. Soltani, T. Knudsen, M. Kragelund, and T. Bak, "Aeolus toolbox for dynamics wind farm model, simulation and control," in *European Wind Energy Conference and Exhibition (EWEC) 2010*. Warsaw, Poland, Tuesday 20 - Friday 23 April 2010: European Wind Energy Association (EWEA), 2010.

[12] "Simplified nrel5mw turbine for simulink," http://www.ict-aeolus.eu/SimWindFarm/model-turbine.html, Control and Automation, Aalborg university, Denmark.

[13] S. Øye, "Tjæreborg wind turbine, 4. dynamic inflow measurement," Technical University of Denmark, Lyngby, Denmark, Tech. Rep. VK-204, 1991.

[14] H. Snel and J. G. Schepers, "Investigation and modelling of dynamic inflow effects," in *European Community Wind Energy Conference*, A. D. Garrad, W. Palz, and S. Scheller, Eds., EEC. H.S. Stephens & Associates, 1993, pp. 371–375.

[15] S. Øye, "Tjæreborg wind turbine, first dynamic inflow measurement," Technical University of Denmark, Lyngby, Denmark, Tech. Rep. VK-189, 1991.

[16] T. Burton, D. Sharpe, N. Jenkins, and E. Bossanyi, *Wind Energy Handbook*. John Wiley, 2008.

[17] I. Munteanu, A. I. Bratcu, N.-A. Cutululis, and E. Ceanga, *Optimal Control of Wind Energy Systems*. Springer, 2008.

[18] A. Papoulis and S. U. Pillai, *Probability, Random Variables and Stochastic Processes*, 4th ed. McGraw-Hill, 2002.

[19] H. Madsen, *Time Series Analysis*. Chapman & Hall, 2008, iSBN: 978-1-4200-5967-0.

[20] E. Bossanyi, A. Wright, and P. Fleming, "Controller field tests on the nrel cart3 turbine," http://www.upwind.eu/publications/5-control-systems.aspx, Project UpWind, Tech. Rep. 11593/BR/09, 200X.